

Article

Design, Synthesis, Structural Insights, Tyrosinase Inhibition, and Sun Protection Factor of New Thiosemicarbazone Derivatives

Sebastiano Masuri ^{1,†} , Benedetta Era ^{2,†} , Francesca Pintus ² , Sonia Floris ², Francesca Meloni ¹ ,
Francesca Pettinau ¹ , Enrico Podda ³ , Maria Grazia Cabiddu ¹ , Antonella Fais ^{2,*}  and Tiziana Pivetta ^{1,*} 

¹ Department of Chemical and Geological Sciences, University of Cagliari, S.S. 554 Bivio Sestu, Monserrato, 09042 Cagliari, Italy; sebastiano.masuri@unica.it (S.M.); francesca.meloni96t@unica.it (F.M.); francesca.pettinau@unica.it (F.P.); mgcabidd@unica.it (M.G.C.)

² Department of Life and Environmental Sciences, University of Cagliari, S.S. 554 Bivio Sestu, Monserrato, 09042 Cagliari, Italy; era@unica.it (B.E.); fpintus@unica.it (F.P.); s.floris@unica.it (S.F.)

³ Centre for Research University Services (CeSAR), University of Cagliari, S.S. 554 Bivio Sestu, Monserrato, 09042 Cagliari, Italy; enrico.podda@unica.it

* Correspondence: fais@unica.it (A.F.); tpivetta@unica.it (T.P.)

† These authors contributed equally to this work.

Abstract: Tyrosinase, a key protein in the biosynthesis of melanin pigments, is crucial in determining skin pigmentation. Inhibiting tyrosinase activity is a promising approach for treating conditions related to excessive pigmentation. For the synthesis of more potent tyrosinase inhibitors, we combined two approaches, para-substitution and lipophilicity, to enhance the inhibitory properties of (*E*)-2-(4-hydroxybenzylidene)hydrazine-1-carbotiamide, whose enzyme inhibitory properties have been previously demonstrated. The newly synthesized compounds showed potent inhibition activity against tyrosinase in the micromolar concentration range. The synthesised compounds were up to 41 times more effective than kojic acid. In addition to this biological activity, all molecules were evaluated for their sun protection factor to determine their photoprotective effects. All the compounds showed higher efficacy than reference compounds, used as sunscreens in photoprotective preparations. All compounds were noncytotoxic at the concentration required to inhibit tyrosinase activity. With the aim of defining the potential binding modes and the kind of interactions between the studied molecules and the catalytic site of mushroom tyrosinase, molecular docking simulations were also performed.

Keywords: thiosemicarbazones; tyrosinase; enzyme inhibition



Citation: Masuri, S.; Era, B.; Pintus, F.; Floris, S.; Meloni, F.; Pettinau, F.; Podda, E.; Cabiddu, M.G.; Fais, A.; Pivetta, T. Design, Synthesis, Structural Insights, Tyrosinase Inhibition, and Sun Protection Factor of New Thiosemicarbazone Derivatives. *Molecules* **2024**, *29*, 5629. <https://doi.org/10.3390/molecules29235629>

Academic Editor: Faiza Diaba

Received: 27 October 2024

Revised: 14 November 2024

Accepted: 25 November 2024

Published: 28 November 2024



Copyright: © 2024 by the authors. Licensee MDPI, Basel, Switzerland. This article is an open access article distributed under the terms and conditions of the Creative Commons Attribution (CC BY) license (<https://creativecommons.org/licenses/by/4.0/>).

1. Introduction

Thiosemicarbazones constitute a class of synthetic organic compounds afforded by the condensation of carbonyl compounds (e.g., aldehydes, ketones) with thiosemicarbazide. These molecules are known for forming stable chelates with different metal ions, thanks to the presence and spatial arrangements of the thiocarbonyl sulphur and hydrazino nitrogen atoms [1,2]. Moreover, many thiosemicarbazones have been evaluated for their anti-tyrosinase properties, observing that these molecules may show potent inhibitory activity towards these macromolecules [3–8].

Tyrosinase (EC 1.14.18.1) (Tyr) is the key enzyme of melanogenesis. Tyr contains copper in the active site and performs two sequential enzymatic reactions using molecular oxygen: the ortho-hydroxylation of monophenols and the oxidation of o-diphenols to the corresponding quinones. The reactive quinones then polymerize spontaneously into melanins [9]. Under normal conditions, melanin protects the skin from UV radiation, but its overproduction can cause hyperpigmentation. Different strategies can be exploited to modulate melanogenesis, including inhibiting tyrosinase activity [10,11]. Various methods have been employed to study the Tyr inhibitory activity of samples over the years [12].

Although numerous studies have identified synthetic and natural tyrosinase inhibitors, many of these potential inhibitors are not widely used due to their lack of efficacy and associated toxicities, such as cytotoxicity.

Numerous advances in the biochemical field have allowed a more detailed and precise study of the mechanism of Tyr inhibition [13–15]. Optimization of the expression and purification of mushroom and human Tyr has allowed the acquisition of more information into inhibiting these tyrosinases [12]. Depending on the research to be developed, the choice of the appropriate enzyme should be essential. Despite this, most of the studies have been based on in vitro inhibition tests using mushroom Tyr [12,16], which is easily available and cheap, despite the low homology between human and mushroom Tyr and the significant differences in their interaction patterns. However, all Tyr sources share similar copper active sites and it is believed that thiosemicarbazones exert their anti-tyrosinase properties by targeting the very two copper cofactors in the enzyme's catalytic site [3–5].

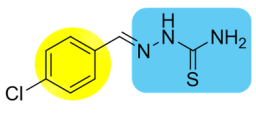
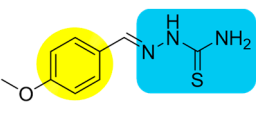
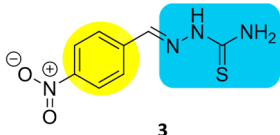
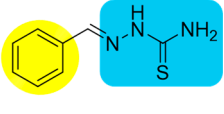
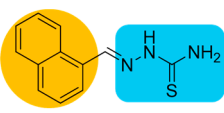
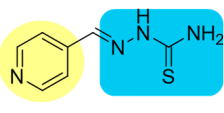
Benzaldehyde-based thiosemicarbazones have proved to possess promising anti-tyrosinase properties. In fact, the introduction of the aromatic ring might increase the affinity between the ligand and the macromolecular target, due to the higher similarity with natural tyrosinase substrates, such as L-Tyrosine and L-dihydroxyphenylalanine (L-DOPA). Moreover, additional hydrophobic interactions with the enzyme's aminoacidic residues might take place [3]. The anti-tyrosinase activity of benzaldehyde-based thiosemicarbazones seems also to be tuneable according to the position of the substituents in the phenyl ring. For instance, para-substituted derivatives proved to be effective tyrosinase inhibitors, with IC_{50} values ranging in the micromolar order [17–20]. Compounds **1** (p-Cl), **2** (p-OCH₃), and **3** (p-NO₂) are reported as examples in Table 1.

Lipophilicity also appears to be important in the modulation of anti-tyrosinase activity. Lee et al. observed how the substitution of the phenyl ring (**4**) with a naphthalene one (**5**) increases the inhibitory activity in B16 melanoma cells (Table 1), while the introduction of a more polar ring, like a pyridyl one in compound **6**, determines a loss of the inhibitory activity ($IC_{50} > 30 \mu\text{M}$). The authors hypothesized that the higher lipophilicity introduced by the naphthalene moiety results in a higher ability of **5** at permeating B16 cell membranes [21].

In this study, we decided to combine the two approaches described above (p-substitution + lipophilicity) with the aim of designing and synthesizing more potent tyrosinase inhibitors. Starting from (E)-2-(4-hydroxybenzylidene)hydrazine-1-carbothioamide (**TC1**, Figure 1), whose enzymatic inhibitory properties were previously reported [20], we functionalized the p-hydroxy group with an alkyl benzenesulfonate moiety (**TCMS1**, Figure 1) and an aryl benzenesulfonate one (compounds **TCBS1-5**, Figure 1). The sulphonate moiety has the main role of linker between the added alkyl/aryl moiety and the pre-existing molecular structure. Additionally, it might also help in stabilizing the adopted bioactive conformation by establishing additional interactions with the surrounding aminoacidic residues of the enzyme. Moreover, we evaluated whether the nature of the substituents could influence the activity of the p-substituted **TCBS2-5** derivatives.

To give an overall view of the characteristics of the synthesized molecules, several chemical, biological, and theoretical studies were carried out, in particular: X-ray diffraction study, Hirshfeld analysis and molecular descriptors calculations, Tyr inhibition, sun protection factor (SPF), cytotoxicity, antioxidant activity, and copper chelation ability. All these experiments were carried out to obtain useful information on the compound stability and the drug-likeness of the studied molecules, to foresee their behaviour in solution or in polar/apolar media and to ascertain the kind of interaction with the tyrosinase enzyme. All these properties are, in fact, all related to a potential use as drug or in cosmetic formulation.

Table 1. Tyrosinase inhibitory activity (using L-DOPA as substrate), expressed as IC_{50} , for p-substituted 1–3 thiosemicarbazones and anti-melanogenesis activity (on B16 melanoma cells), reported as IC_{50} , expressed as a function of lipophilicity for 4–6 thiosemicarbazones.

Molecule	Tyrosinase Inhibitory Activity IC_{50} (μ M)	Anti-Melanogenesis Activity IC_{50} (μ M)	cLogP	References
 1	0.84 1.9	-	-	[17,18]
 2	0.44 1.48	-	-	[17,20]
 3	1.9	-	-	[19]
 4	-	>10	1.865	[21]
 5	-	1.1	3.039	[21]
 6	-	>30	1.088	[21]

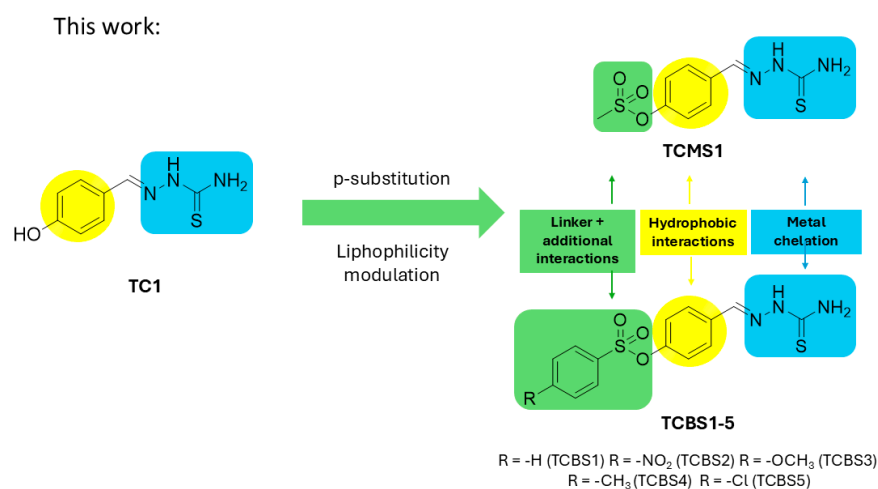
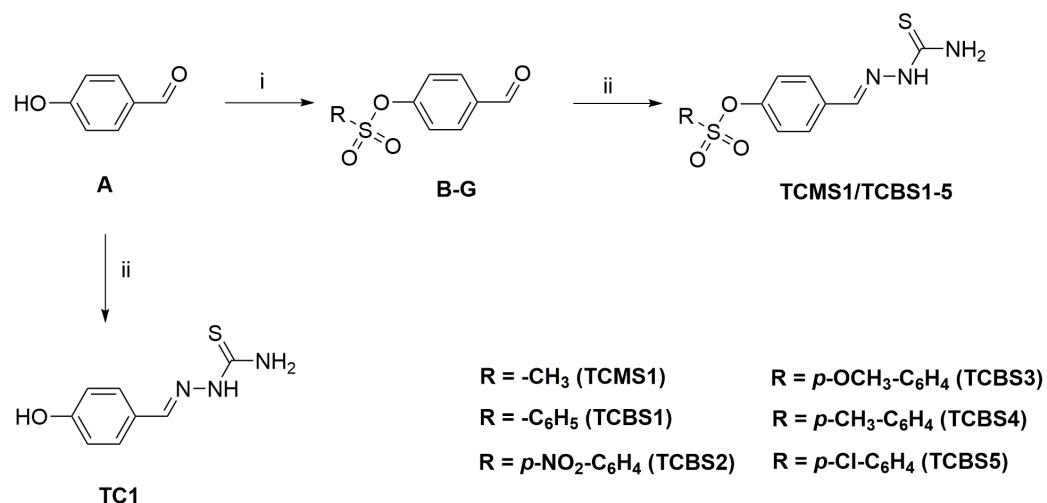


Figure 1. Design strategy and molecular structures of the thiosemicarbazone derivatives proposed in this work.

2. Results and Discussion

2.1. Synthesis and Chemical Characterisation

Target compounds **TCMS1** and **TCBS1-5** were easily synthesized (Scheme 1) by reacting 4-hydroxybenzaldehyde (**A**) with the corresponding aryl sulfonyl chlorides, affording the aryl sulfonate intermediates **B–G**. These compounds (as crudes) were then converted to the desired thiosemicarbazones in the presence of a catalytic amount of acetic acid. The reference molecule **TC1** was obtained by directly converting **A** to the correspondent thiosemicarbazone derivative, using the synthetic approach just discussed. The yields of the final products ranged from moderate to good. To our knowledge, compounds **TCMS1** and **TCBS1-5** have been used as intermediates for the preparation of enzymatic inhibitors (e.g., towards glucosidase, carbonic anhydrase, acetylcholine esterase, butyrylcholine esterase), but their chemical characterization has not been performed [22,23]. For this reason, we characterized the **TCMS1** and **TCBS1-5** molecules employing different techniques (melting point, NMR, HR-ESI-MS). In the $^1\text{H-NMR}$ spectra of all the reported compounds, characteristic broad singlets from $-\text{NH}$ and $-\text{NH}_2$ protons were visible. Their chemical shift values were in accordance with those reported for **TC1** and other structurally related thiosemicarbazones [19,20,24,25]. The $-\text{NH}$ protons were highly de-shielded and fell in the 10.5 ÷ 11.5 ppm range since they were included in a highly conjugated structure. The $-\text{NH}_2$ protons typically showed up as two separate broad singlets around 8 ppm due to their magnetic inequivalence. This behaviour can be attributed to the partially restricted rotation around the C-N bond due to the mesomeric effect [25], as well as the potential intramolecular hydrogen bonding between one of the NH_2 hydrogens and the sp^2 (imino) nitrogen, which resulted in the formation of a five-membered ring. In order to further prove the nature of these hydrogens, we performed a hydrogen exchange experiment by recording the $^1\text{H NMR}$ spectrum of **TCBS5** in deuterated acetone before (Figure S12) and after (Figure S14) the addition of D_2O . As can be seen, addition of deuterium oxide determined a hydrogen/deuterium exchange, which resulted in the disappearance of the aforementioned signals.



Scheme 1. Reaction schemes and structures of the synthesized compounds. Reaction conditions were (i) $\text{R-SO}_2\text{Cl}$, triethylamine, dichloromethane, r.t. overnight; (ii) thiosemicarbazide, absolute ethanol, glacial acetic acid, rf 6 h.

Interestingly, the positive HR-ESI-MS spectra of the **TCMS1** and **TCBS1-5** molecules showed a peak at $M+17$ mass-to-charge ratio (m/z), corresponding to the protonated S-oxide derivative obtained in the ESI phase. Redox phenomena in positive ESI-MS were already observed for many classes of organic ligands and metal complexes depending on experimental conditions (solvent, needle voltage, housing temperature, etc.) [26–31]. The parent ions at $M+17$ m/z showed a common loss of 18 Da, corresponding to a water

molecule. When the spectra of the same compounds were recorded in negative mode (absence of an oxidizing environment), the analytes did not undergo any redox phenomena and were visible as deprotonated molecular ions ($[M-H]^-$) or chlorinated adducts ($[M+Cl]^-$). HR-ESI mass spectra in both positive and negative mode for compound **TCMS1** are shown in the Supplementary Material (Figures S15 and S16) as an example. The crystal structure of the **TCBS1** was determined by means of single-crystal X-ray diffraction (SC-XRD).

2.2. Crystal Structure

Single crystals of **TCBS1** were successfully grown by slow evaporation from chloroform. SC-XRD analysis of a colourless needle-shaped crystal confirmed the nature and chemical connectivity of **TCBS1** that crystallized in the triclinic $P1^-$ space group with two crystallographically independent molecules in the asymmetric unit (Figure 2, Table S1).

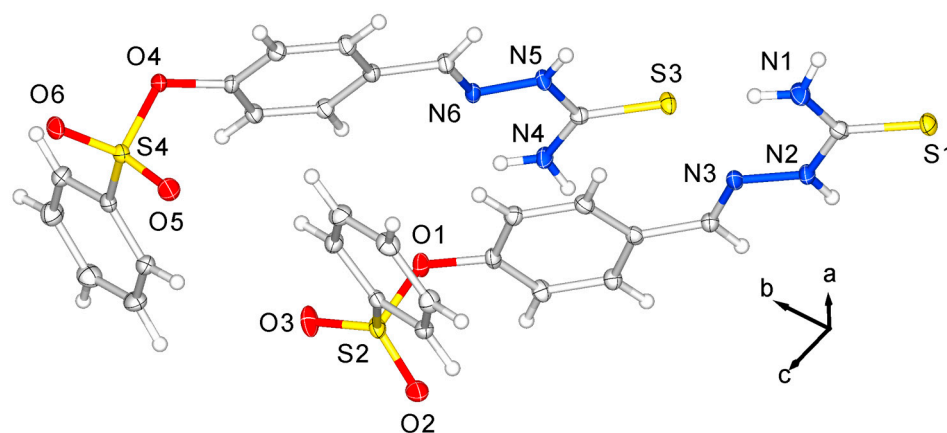


Figure 2. X-ray crystal structure of **TCBS1** showing the heteroatoms' labelling scheme adopted. Displacement ellipsoids are drawn at the 50% probability level.

Thiosemicarbazone moieties in the two molecules of **TCBS1** were coplanar with the plane defined by the vicinal aromatic ring and were in excellent agreement with the geometrical parameters found in this family of structurally characterized derivatives deposited at the CSD (Table S2). On the other hand, the main conformational differences were observed for the dihedral angles C–S–O–C being about 68 and 79° (for C9–S2–O1–C6 and C23–S4–O4–C20, respectively) and for the angle between the planes defined by the two aromatic rings belonging to the same **TCBS1** molecule being about 60 and 82°, respectively. Both molecules of **TCBS1** interacted via N–H...S between the sulphur atom and both the amines of the thiosemicarbazone moieties defining a set of $R_2^2(8)$ hydrogen-bonding motifs [32] that led to the formation of undulated ribbons developing along the a-axis (Figure S17). The two crystallographically independent molecules of **TCBS1** are depicted as units A (light blue) and B (green) according to Figure S17 and Table S5. The crystal packing was further decorated by slipped π - π stacking interactions between the aromatic rings of the tosyl groups belonging to different units (Figure S18), increasing the dimensionality of the final network (Figure S19).

2.3. Hirshfeld Surface

Hirshfeld surface (HS) analysis is a modern and powerful tool to analyse the intermolecular interactions present inside the crystal by a simple 3D visualization [33–35]. HSs are mapped with respect to four principal parameters, i.e., d_{norm} (Figure 3a), shape index (Figure 3b), curvedness (Figure 3c), and void (Figure 4). In the d_{norm} surface, white, red, and blue areas represent contacts close to, shorter than, and longer than the sum of the van der Waals radii, respectively [36–38]; the red circles on the surface are indicative of the hydrogen bonding between S1 or S3 sulphur atoms (H acceptors) and the NH groups

of neighbouring molecules. The size of the red circle is related to the strength of the interactions, with distance varying from 2.303 Å of S3-HN5 to 2.497 Å of S1-HN1.

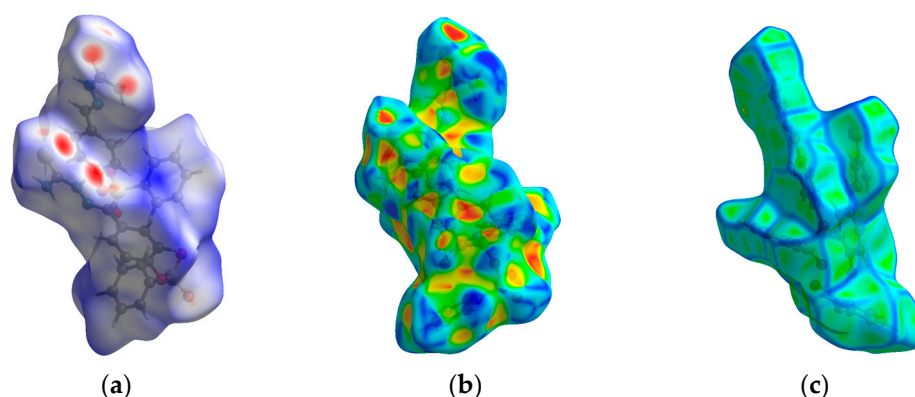


Figure 3. HSs mapped with (a) $dnorm$ in the range of -0.4171 a.u. (red) to 1.6374 (blue); (b) shape index showing red and blue triangles indicating the π - π stacking areas and (c) curvedness with flat areas highlighting the ring contribution in π - π stacking interactions.

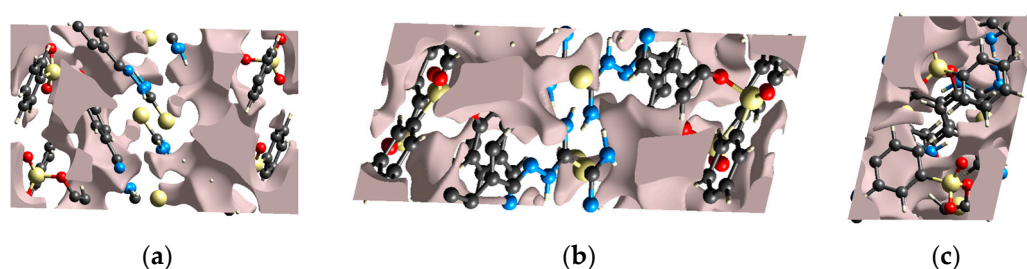


Figure 4. Graphical views of voids in the crystal packing of TCBS1, along the projections of [100] (a), [010] (b), and [001] (c). Void volume is 188.45 \AA^3 .

The HSs mapped over shape index (Figure 3b) and curvedness (Figure 3b) are useful to describe the effect of weak intermolecular interactions in the crystal. The shape index surface showed complementary depressions indicating the contact areas between two Hirshfeld surfaces [39–42]. In this map, adjacent red and blue triangular regions are consistent with the presence of π - π stacking: the red triangles are concave zones related to the π - π stacked rings located above, while the blue triangles are convex zones representative of the aromatic rings within the surface. The last map, plotted over the curvedness, depicts the planarity and the sharp edges within the surface. The blue zones are related to the curved surface and large blue areas are indicative of strong hydrogen bonding interactions. The flat zones are due to weak and low-energy interactions [39].

The HS mapped over the void [43,44] shows regions with low electron density. The calculated void volume occupies 12.2% of the total volume of the unit cell, indicating a not rigid crystal packing.

In conclusion, $dnorm$ and curvedness parameters accounted for close and long contacts, π - π stacking, and hydrogen bonding. All these features were involved in the chemical and biochemical reactivity, affecting also the solubility of the compound in different media (polar or apolar). The void percentage is an index of the softness or hardness of the crystal, and this information is useful in the preparation of formulations where the compound could be present in a dispersed phase.

2.4. Molecular Descriptors

The preliminary evaluation of the drug-likeness of the studied molecules was performed by means of different molecular descriptors. Results are summarized in Table 2. All the compounds here reported adhered to the Lipinski's rule of five [45] and showed

TPSA values (sum of the surface occupied by polar functional groups) of (i) lower (or almost equal in the case of **TCBS2**) than the upper limit of 140 \AA^2 , symptomatic of an oral bioavailability from good to moderate, and (ii) higher than 60 \AA^2 , indicative of a modest blood–brain barrier (BBB) permeability [46,47].

Table 2. Calculated molecular descriptors for the studied compounds.

	TC1	TCMS1	TCBS1	TCBS2	TCBS3	TCBS4	TCBS5
miLogP ^a	1.40	1.31	2.85	2.81	2.90	3.30	3.52
TPSA (\AA^2) ^b	70.64	93.79	93.79	139.61	103.02	93.79	93.79
n-atoms ^c	13	17	22	25	24	23	23
MW (Da)	195.25	273.34	335.41	380.41	365.44	349.44	369.86
n-ON ^d	4	5	5	7	6	5	5
n-OHNH ^e	4	3	3	3	3	3	3
n-violations ^f	0	0	0	0	0	0	0
n-rotb ^g	3	5	6	7	7	6	6
volume (\AA^3) ^h	166.87	215.83	270.68	294.01	296.23	287.24	284.22

^a Calculated logarithm of the partition coefficient between n-octanol and water (miLogP); ^b topological polar surface area (TPSA); ^c number of atoms in the molecule (n-atoms); ^d number of hydrogen bond acceptors (n-ON); ^e number of hydrogen bond donors (n-OHNH); ^f number of violations of the Lipinski's rule of five; ^g number of rotatable bonds (n-rotb); ^h molecular volume.

2.5. Tyrosinase Inhibition

All compounds were evaluated for their inhibitory effect on the tyrosinase enzyme. As can be observed in Table 3, all the tested compounds were found to be significantly more effective than kojic acid. **TC1** had a significantly higher IC_{50} value than other compounds in the series, being only 2.5 times more effective than kojic acid, while the other compounds were up to 41 times more effective than the standard inhibitor.

Table 3. Half maximal inhibitory concentration (IC_{50}) values of **TC1**, **TCMS1**, and **TCBS1-5** compounds against mushroom tyrosinase activity (data are given as mean \pm standard deviation (SD) of triplicate experiments).

Compound	$IC_{50} \text{ \mu M}^*$
TC1	7.1 ± 0.2^a
TCMS1	1.6 ± 0.02^b
TCBS1	0.44 ± 0.03^b
TCBS2	0.66 ± 0.05^b
TCBS3	0.44 ± 0.01^b
TCBS4	0.44 ± 0.01^b
TCBS5	0.71 ± 0.02^b
Kojic acid	18 ± 1^c [48]

* Different letters indicate statistically significant differences between compounds ($p < 0.001$).

The results highlighted that the functionalization of the hydroxyl group of **TC1** with a $-\text{SO}_2\text{R}$ moiety plays a crucial role in enhancing the anti-tyrosinase activity. Specifically, the $-\text{SO}_2\text{R}$ modification appeared to facilitate better binding to the enzyme's active site. Furthermore, replacing a methyl (**TCMS1**) with a more lipophilic phenyl group in derivatives such as **TCBS1-5** did not significantly reduce the IC_{50} value. The inhibitory activity did not appear to be influenced by the presence and nature of the substituents in the para position of the phenylsulfonyl moiety (**TCBS1-5**). All these considerations suggest that, among the structural modifications made in the studied compounds, introducing sulfonyl groups could be a promising strategy to improve the efficacy of tyrosinase inhibitors.

2.6. Antioxidant Activity

Two methods, with DPPH and ABTS, were used to evaluate the antioxidant activity of the synthesized compounds, resulting in similar values for each compound analysed (see Table 4).

Table 4. Free radical scavenging activity (TC1, TCMS1, and TCBS1-5) as a percentage of inhibition of free radicals (I). The data of triplicate experiments are given as mean \pm standard deviation (SD).

Compound	DPPH (% I \pm SD)	ABTS (% I \pm SD)
TC1	74 \pm 3	74 \pm 1
TCMS1	20 \pm 2	42 \pm 4
TCBS1	26 \pm 2	39 \pm 1
TCBS2	16 \pm 2	25 \pm 4
TCBS3	33 \pm 4	35 \pm 1
TCBS4	20 \pm 1	30 \pm 2
TCBS5	32 \pm 5	22 \pm 2

As shown in Table 4, the tests highlighted an antioxidant power between 16% and 74% among the compounds examined. Compound TC1, which has a hydroxyl group, showed the highest value.

2.7. Sun Protection Factor

In addition to all the biological activities examined, all molecules were evaluated for their sun protection factor (SPF) to determine their skin photoprotective effects. Determining the SPF value of compounds with possible skin application could be important since UV rays trigger oxidative stress reactions and progressive skin aging. The SPF values are reported in Table 5. The studied compounds were compared to caffeic acid (CA), ferulic acid (FA), and cinnamic acid (CI), natural components that are used as sunscreens in photoprotective preparations [49], resulting as being more effective.

Table 5. Sun protection factor (SPF) values of thiosemicarbazone derivates (TC1, TCMS1, TCBS1-5 compounds) and ferulic acid (FA), caffeic acid (CA), and cinnamic acid (CI).

Compound	SPF *
TC1	11.0 \pm 0.4 ^{a,b}
TCMS1	11 \pm 2 ^{a,b}
TCBS1	11 \pm 2 ^{a,b}
TCBS2	13 \pm 2 ^a
TCBS3	10 \pm 2 ^{a,b}
TCBS4	14 \pm 2 ^a
TCBS5	11 \pm 2 ^{a,b}
FA #	7.5 \pm 0.2 ^b
CA #	6.6 \pm 0.4 ^b
CI #	2.0 \pm 0.2 ^d

* Different letters indicate statistically significant differences between compounds ($p < 0.001$). # Data taken from reference [49].

2.8. Copper Chelation Studies

It is well known that Cu(II), as borderline species according to Hard and Soft Acid and Basis Theory (HSAB), can form stable metal complexes with both hard donors (e.g., oxygen) and soft ones (e.g., sulphur) [50]. Many bioactive Cu(II) complexes bearing sulphur-containing functional groups (e.g., thioamides, thiosemicarbazones) or oxygen-based donors (e.g., polyphenols, carboxylates) have been studied at both solution and solid states [51–54]. Hence, the design of tyrosinase inhibitors having metal chelating groups might be useful thanks to their capability to target the enzyme's metal cofactors. Based on these premises, we aimed to preliminarily evaluate the capability of the studied

molecules to form copper complexes in solution at the same pH used for enzymatic inhibition experiments (6.8), using Job's method. We selected compound **TCBS4** as a model for the copper chelation study. The Job's Plots (Figure S20A,B), carried out for this molecule, were obtained from absorbance data recorded at 310 and 318 nm (Figure S20C). The experimental results evidenced the formation of a 1:3 (metal:ligand) complex ($\chi_L = 0.75$). Uncorrected absorbance data as a function of ligand's molar fraction are also shown (Figure S21). It is important to note that these results refer to the metal chelating capabilities of **TCBS4** in a model solution containing Cu^{2+} ions (derived from Cu(II) chloride). In tyrosinase's catalytic site, the two metal ions were already coordinated by six histidine residues (three for each metal ion). Hence, based on these data, we can assume that the studied molecules might interact with the two metal cofactors by forming mixed complexes with different molar ratios, due to the steric hindrance introduced by the surrounding residues in the enzyme's catalytic site. This hypothesis seems to be corroborated by molecular theoretical simulations (See Section 2.10).

2.9. Cytotoxicity Analysis

Based on the promising results from earlier experiments, we conducted further evaluations to determine the compounds' biosafety effectiveness. The results are depicted in Figure 5. Our findings demonstrated that all compounds were noncytotoxic to HaCaT cells at the concentration required to inhibit tyrosinase activity.

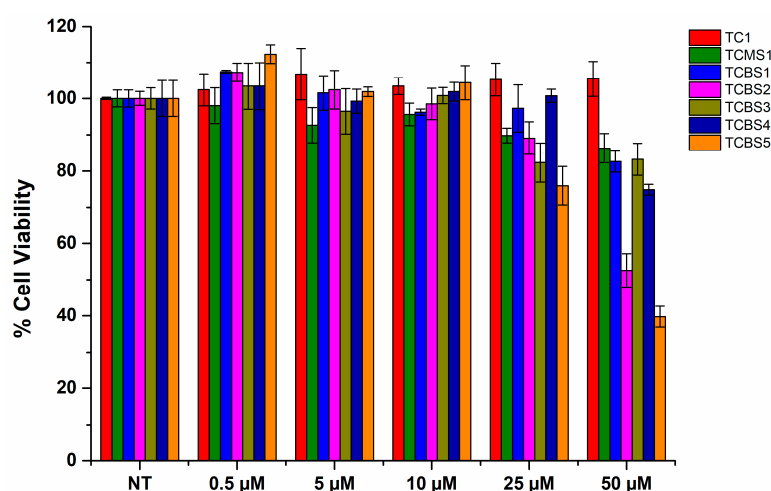


Figure 5. Cell viability of HaCaT cell line after treatment with different concentrations of compounds. Concentrations were from 0 (NT) to 50 μM .

2.10. Molecular Docking

With the aim of assessing the potential binding modes and interactions of the studied molecules in the catalytic site of mushroom tyrosinase (MTa), molecular docking simulations were performed starting from the X-ray structure of the complex (PDB: 2Y9X) between mushroom tyrosinase (from *Agaricus bisporus*) and the natural inhibitor tropolone (OTR). As previously reported [55], the suitability of the computational protocol was verified by redocking the cognate OTR ligand in the enzyme's binding pocket, affording an acceptable root mean square deviation (RMSD) between the atomic positions of docked and crystallized ligands (2.3 Å). Docking scores and intermolecular interactions are summarized in Table S6. All the studied thiosemicarbazones fit the catalytic site of mushroom tyrosinase, showing two possible binding orientations. In the case of compound **TC1** (Figure 6), its docked pose projected the thiosemicarbazone group towards the enzyme's outer surface with the p-hydroxyphenyl ring collocated in the enzyme's binding pocket. This conformation was further stabilized by a hydrogen bond between the ligand's hydrazido nitrogen and the Gly-281 residue (D-H...A distance: 2.01 Å) and by π - π stacked interactions with the Hys-263 ring (centroid distance: 3.89 Å), as shown in Figure S22.

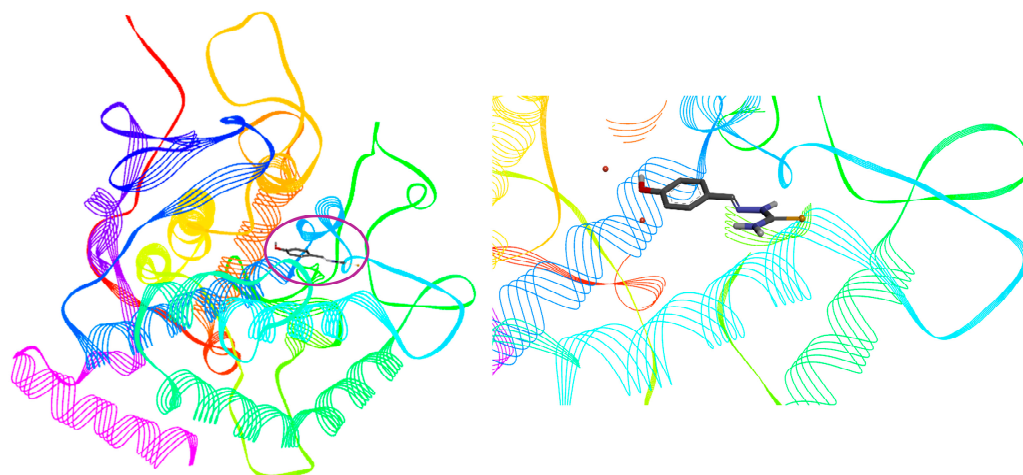


Figure 6. Full (left) and zoomed (right) view of the highest-rated docked pose of compound TC1 in the MTa site.

In the opposite, when the hydroxyl group was functionalized with a $-SO_2R$ moiety, as in **TCMS1** and **TCBS1-5**, their docked poses underwent a 180° twist, with their thiosemicarbazone groups involved in the coordination of the two copper ions through the ligands' sulphur atoms (Figures 7 and S23). The conformations of all the thiosemicarbazones were further stabilized by a series of hydrophobic interactions, as observed from a lipophilic analysis of the enzyme's surrounding residues. In particular, all of them shared hydrophobic interactions between the ligands' phenyl ring (bonded to the thiosemicarbazone group) and the Val-283 (Figure S24). This residue was involved in stabilizing the bioactive conformation of the tropolone molecule in the 2Y9X complex [55–57]. In addition, molecular docking simulations of different inhibitors in the catalytic site of mushroom tyrosinase showed an involvement of the Val-283 residue as well [7,55,57–60]. Substitution of the methylsulfonyl fragment in **TCMS1** with a more lipophilic phenylsulfonyl one, as in **TCBS1-5**, led to additional hydrophobic interactions between this phenyl ring and the aminoacidic residues Val-248 and Phe-264. These findings might help in explaining the similar anti-tyrosinase potency of the phenyl (**TCBS1-5**) thiosemicarbazone derivatives.

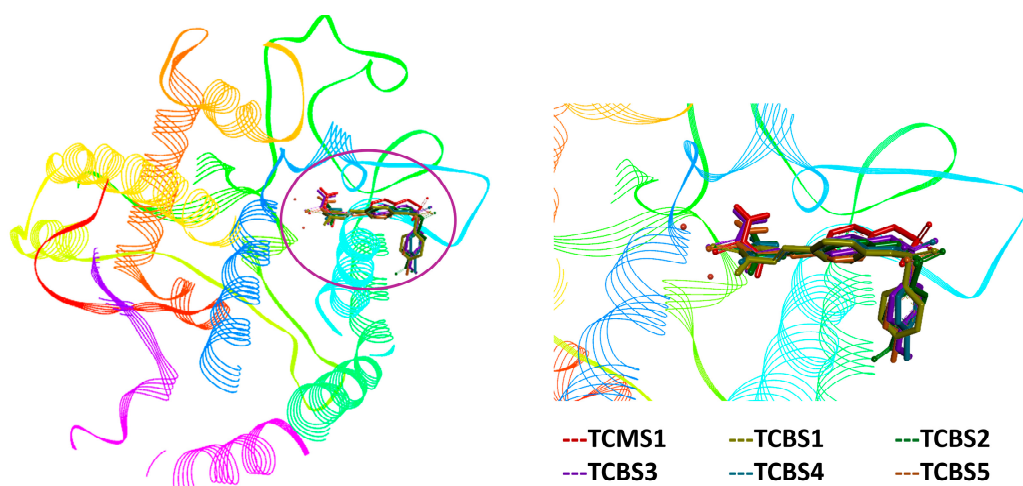


Figure 7. Full (left) and zoomed (right) view of the highest-rated docked poses of compounds **TCMS1**, **TCBS1-5** in the catalytic site of mushroom tyrosinase.

3. Materials and Methods

3.1. Chemicals

The 4-hydroxybenzaldehyde was purchased from Eastman Organic Chemicals (Kingport, TN, USA). Absolute ethanol, dichloromethane, sodium sulphate, copper(II) chloride, triethylamine, thiosemicarbazide, p-chlorobenzenesulfonyl chloride, p-toluenesulfonyl chloride, methanesulfonyl chloride, p-nitrobenzenesulfonyl chloride, isopropanol, acetonitrile, methanol, deuterated dimethyl sulfoxide (DMSO d-6), deuterium oxide (D₂O), deuterated acetone (Acetone d-6), and 2,2'-azino-bis(3-ethylbenzothiazoline-6-sulfonic acid (ABTS) were purchased from Merck (Milan, Italy). The 4-methoxybenzenesulfonyl chloride, sodium dihydrogen phosphate, sodium hydrogen phosphate, and glacial acetic acid were purchased from Thermo Fischer (Kandel, Germany). Benzenesulfonyl chloride was purchased from TCI Europe (Zwijndrecht, Belgium).

3.2. Instrumentation Techniques

Melting points were measured on a Kofler Hot Stage (Rochford, UK) and were uncorrected. Proton and Carbon-13 NMR spectra were acquired with a Bruker Advance III HD 600 spectrometer (Rheinstetten, Germany) at room temperature with tetramethylsilane (TMS) as the internal standard in DMSO-d₆ or Acetone d-6. Low-resolution ESI mass spectra were acquired with a triple quadrupole (QqQ) Varian 310-MS mass spectrometer (Palo Alto, CA, USA) using previously optimized parameters [61]. High-resolution ESI mass spectra were registered on a ThermoFisher ORBITRAP-ELITE instrument (Waltham, MA, USA). The fitting of the isotopic patterns was verified using the mmass 5.5.0 software package [62,63]. UV-vis spectra were recorded using an Agilent Cary 60 spectrophotometer (Palo Alto, CA, USA) with a 1.0 cm quartz cuvette.

3.3. General Procedure for the Synthesis of Intermediates B–G

Compounds B–G (Scheme 1) were synthesized by adapting a previously reported method [64]. In brief, to a suspension of *p*-hydroxybenzaldehyde (2.0 mmol, 1 eq) in dichloromethane (8.0 mL) was added at room temperature triethylamine (2.4 mmol, 1.2 eq) followed by the proper sulphonyl chloride derivative (4.0 mmol, 1 eq). The mixture was left under stirring overnight at room temperature, then treated with a saturated aqueous solution of sodium bicarbonate. The organic phase was separated, and the aqueous layer was extracted multiple times with dichloromethane. The combined organic phases were dried over sodium sulphate and evaporated, affording the desired B–G intermediates as solids. The compounds were used as such for the subsequent step, with no further purification procedures.

3.4. General Procedure for the Synthesis of Target Compounds TC1, TCMS1, TCBS1-5

The proper aldehyde derivative A–G (1.9 mmoles, 1 eq) was dissolved in ethanol (7.6 mL), then thiosemicarbazide (1.9 mmoles, 1 eq) and glacial acetic acid (0.095 mL) were added. The reaction mixture was refluxed for 6 hrs, then cooled to room temperature, affording a solid that was recovered by filtration. Recrystallization from isopropanol (TC1), acetonitrile (TCMS1, TCBS2), methanol (TCBS1), or ethanol (TCBS3-5) afforded the desired products as solids.

(*E*)-2-(4-hydroxybenzylidene)hydrazine-1-carbothioamide (TC1). Yield: 81%. Experimental results were following those reported in the literature [65], m.p. 221–223 °C; ¹H NMR (600 MHz, DMSO-d₆, Figure S1): δ 11.23 (s, 1H), 9.84 (s, 1H), 8.04 (s, 1H), 7.95 (s, 1H), 7.81 (s, 1H), 7.63–7.58 (m, 2H), 6.80–6.75 (m, 2H); LR-ESI-MS (*m/z*) found (calculated): 196.3 (196.0) [M+H]⁺, 217.7 (218.0) [M+Na]⁺.

(*E*)-4-((2-carbamothioylhydrazineylidene)methyl)phenyl methanesulfonate (TCMS1). Yield: 78%; m.p. 224–226 °C; ¹H NMR (600 MHz, DMSO-d₆, Figure S2) δ 11.48 (s, 1H), 8.23 (s, 1H), 8.06 (s, 2H), 7.95–7.90 (m, 2H), 7.40–7.34 (m, 2H), 3.40 (s, 3H); ¹³C NMR (151 MHz, DMSO d₆, Figure S3) δ 178.1, 149.9, 140.8, 133.4, 129.0, 122.5, 37.5; HR-ESI-MS (*m/z*),

found (calculated): 272.0141 (272.0164) $[M-H]^-$, 290.0285 (290.0269) $[M_{S-Ox}+H]^+$ (oxidized product).

(*E*)-4-((2-carbamothioylhydrazineylidene)methyl)phenyl benzenesulfonate (**TCBS1**). Yield: 63%; m.p. 159–160 °C; 1H NMR (600 MHz, Acetone- d_6 , Figure S4) δ 10.49 (s, 1H), 8.14 (s, 1H), 7.91 (s, 1H), 7.89–7.87 (m, 2H), 7.84–7.78 (m, 3H), 7.68 (t, $J = 7.7$ Hz, 2H), 7.50 (s, 1H), 7.07 (d, $J = 8.5$ Hz, 2H); ^{13}C NMR (151 MHz, Acetone d_6 , Figure S5) δ 180.7, 151.4, 141.7, 136.1, 135.6, 134.5, 130.5, 129.5, 129.3, 123.5; HR-ESI-MS (m/z), found (calculated): 334.0305 (334.0320) $[M-H]^-$, 370.0066 (370.0087) $[M+Cl]^-$ with the expected isotopic pattern, 352.0450 (352.0426) $[M_{S-Ox}+H]^+$ (oxidized product).

(*E*)-4-((2-carbamothioylhydrazineylidene)methyl)phenyl 4-nitrobenzenesulfonate (**TCBS2**). Yield: 61%; m.p. 226–228 °C; 1H NMR (600 MHz, DMSO- d_6 , Figure S6) δ 11.47 (s, 1H), 8.48–8.43 (m, 2H), 8.23 (s, 1H), 8.21–8.14 (m, 2H), 8.04 (s, 1H), 8.00 (s, 1H), 7.87–7.82 (m, 2H), 7.13–7.08 (m, 2H); ^{13}C NMR (151 MHz, DMSO d_6 , Figure S7) δ 178.2, 151.1, 149.3, 140.4, 139.4, 133.9, 130.1, 129.0, 125.0, 122.4; HR-ESI-MS (m/z), found (calculated): 379.0145 (379.0171) $[M-H]^-$, 414.9907 (414.9938) $[M+Cl]^-$ with the expected isotopic pattern, 397.0312 (397.0277) $[M_{S-Ox}+H]^+$ (oxidized product).

(*E*)-4-((2-carbamothioylhydrazineylidene)methyl)phenyl 4-methoxybenzenesulfonate (**TCBS3**). Yield: 48%; m.p. 154–156 °C; 1H NMR (600 MHz, Acetone- d_6 , Figure S8) δ 10.50 (s, 1H), 8.14 (s, 1H), 7.91 (s, 1H), 7.82–7.76 (m, 4H), 7.50 (s, 1H), 7.18–7.13 (m, 2H), 7.08–7.03 (m, 2H), 3.93 (s, 3H); ^{13}C NMR (151 MHz, Acetone d_6 , Figure S9) δ 180.7, 165.4, 151.6, 141.8, 134.3, 131.7, 129.5, 127.3, 123.6, 115.6, 56.4; HR-ESI-MS (m/z), found (calculated): 364.0406 (364.0426) $[M-H]^-$, 400.0162 (400.0193) $[M+Cl]^-$ with the expected isotopic pattern, 382.0562 (382.0531) $[M_{S-Ox}+H]^+$ (oxidized product).

(*E*)-4-((2-carbamothioylhydrazineylidene)methyl)phenyl 4-methylbenzenesulfonate (**TCBS4**). Yield: 76%; m.p. 195–197 °C; 1H NMR (600 MHz, Acetone- d_6 , Figure S10) δ 10.49 (s, 1H), 8.13 (s, 1H), 7.90 (s, 1H), 7.83–7.77 (m, 2H), 7.76–7.72 (m, 2H), 7.52–7.46 (m, 3H), 7.09–7.04 (m, 2H), 2.46 (s, 3H); ^{13}C NMR (151 MHz, Acetone d_6 , Figure S11) δ 180.7, 151.5, 146.9, 141.8, 134.4, 133.2, 130.9, 129.5, 129.3, 123.5, 21.6; HR-ESI-MS (m/z), found (calculated): 348.0454 (348.0477) $[M-H]^-$, 384.0214 (384.0243) $[M+Cl]^-$ with the expected isotopic pattern, 366.0608 (366.0582) $[M_{S-Ox}+H]^+$ (oxidized product).

(*E*)-4-((2-carbamothioylhydrazineylidene)methyl)phenyl 4-chlorobenzenesulfonate (**TCBS5**). Yield: 76%; m.p. 194–196 °C; 1H NMR (600 MHz, Acetone- d_6 , Figure S12) δ 10.47 (s, 1H), 8.14 (s, 1H), 7.92–7.86 (m, 3H), 7.85–7.80 (m, 2H), 7.75–7.70 (m, 2H), 7.49 (s, 1H), 7.13–7.07 (m, 2H); ^{13}C NMR (151 MHz, Acetone d_6 , Figure S13) δ 180.7, 151.2, 141.7, 141.6, 134.7, 134.6, 131.1, 130.7, 129.6, 123.5; HR-ESI-MS (m/z), found (calculated): 367.9898 (367.9930) $[M-H]^-$ with the expected isotopic pattern, 403.9659 (403.9697) $[M+Cl]^-$ with the expected isotopic pattern, 386.0067 (386.0036) $[M_{S-Ox}+H]^+$ (oxidized product) with the expected isotopic pattern.

3.5. Crystal Structure

Single-crystal X-ray diffraction data of **TCBS1** were collected at 100 K on a Bruker D8 Venture diffractometer equipped with a PHOTON II detector. The structure was solved with the ShelXT [66] solution program using dual methods and developed by iterative cycles of least-squares refinement on F2 using ShelXL 2018/3 [66]. Olex2 1.5 [67] was used as the graphical interface and for the preparation of figures. Hydrogen atoms were placed geometrically and refined isotropically riding on their parent C atom with $U_{iso}(H) = 1.2U_{eq}(C)$. H atoms bonded to heteroatoms were located from the difference Fourier map and their positions were refined freely. Crystallographic data were deposited at the Cambridge Crystallographic Data Center (CCDC) under deposition number: 2374503. These data can be obtained free of charge at: <https://www.ccdc.cam.ac.uk/structures>.

3.6. Hirshfeld Analysis

Hirshfeld analysis was carried out on structural data with Crystal Explorer software (v. 21.5, Rev. 608bb.32) [32].

3.7. Molecular Descriptors

All the calculations were performed using the Molinspiration property engine (v2022.08, accessed on 16 May 2024).

3.8. Tyrosinase Inhibition Assay

Mushroom Tyr inhibition was assessed as described previously [11] with minor modifications. A solution consisting of 50 mM of phosphoric acid buffer (pH 6.8), mushroom tyrosinase solution (Sigma Chemical Co., Milan, Italy) at a final concentration of 72 U/mL, and DMSO or the compounds tested was incubated at 37 °C for 10 min; L-DOPA was then added and the dopachrome formation was monitored at 492 nm. The measurements were taken using a FLUOstar OPTIMA (BMG Labtech, Offenburg, Germany). The IC₅₀ value was determined by analysing dose–response curves. Kojic acid was used as a reference tyrosinase inhibitor.

3.9. Antioxidant Assays

3.9.1. DPPH

Radical scavenging activity of the thiosemicarbazone derivatives was estimated according to the previously reported method [68] with slight modification using the stable DPPH radical. A solution of 0.1 mM DPPH radical was added to various concentrations of the compounds. The absorbance of the DPPH radical without an antioxidant, i.e., blank, was also measured. The mixture was shaken vigorously and kept at room temperature for 30 min in the dark. The absorbance of the reaction mixture was measured at 517 nm spectrophotometrically. All the determinations were performed in triplicate.

3.9.2. ABTS

Samples of each compound (10 µL) were added to 990 µL of ABTS, and the reduction in the blue-green radical ABTS^{•+} by hydrogen-donating antioxidants was evaluated by measuring the absorbance at 734 nm after 1 min of incubation. All the measurements were carried out at least three times.

3.10. Sun Protection Factor (SPF)

The sun protection factor of thiosemicarbazone derivatives was measured by the UV absorbance method, as previously reported [11]. The absorbances of the compounds (50 µM) were recorded in the range of 290–320 nm, with 5 nm increments, and three measurements were performed at each point. The SPF was calculated by using the Mansur Equation:

$$SPF = CF \times \sum_{320}^{290} EE(\lambda) \times I(\lambda) \times Abs(\lambda)$$

where *CF* = correction factor (10); *EE* (λ) = erythemogenic effect of radiation with wavelength λ ; *I*(λ) = solar intensity spectrum; and *Abs*(λ) = spectrophotometric absorbance values at wavelength λ . The values of *EE* (λ) \times *I*(λ) are constant, as determined by Sayre et al. [69].

3.11. Copper Chelation Studies

Stock solutions of **TCBS4** and Copper(II) chloride dihydrate 3.20 mM were prepared in DMSO, then diluted to 32 µM in 50 mM Phosphate buffer pH 6.8 (percentage of DMSO in the diluted solutions \approx 1%). Eleven solutions having a variable molar ratio of the two components (from 0:10 to 10:0) but fixed final volume (2.0 mL) and total molar concentration (32 µM) were prepared, and the UV-vis spectra were recorded in the 250–500 nm range. Absorbance data were corrected from the contribution of the pure reactants.

3.12. Cell Viability Assay

The cellular cytotoxicity of compounds was investigated using a 3-(4,5-dimethylthiazol-2-yl)-2,5-diphenyl-tetrazolium bromide (MTT) assay [70]. The HaCaT cell line of human keratinocytes was obtained from CLS-Cell Line Services in Eppelheim, Germany. The cells were exposed for 24 h to compounds at concentrations ranging from 0.5 to 50 μ M. Then, MTT reagent (0.5 mg/mL in DMEM) was added to each well. The plate was incubated for 3 h at 37 °C. The MTT solution was removed from the culture plate, and 100 μ L of DMSO solvent was added to solubilize the water-insoluble formazan crystals formed in the cells. The absorbance was determined at 570 nm using a microplate reader (VANTASTAR_BMG LABTECH GmbH, Offenburg, Germany).

3.13. Docking Calculations

Molecular docking simulations were performed using the CCDC GOLD software (v2024.1.0, Cambridge, UK) [71]. The crystal structure of the adduct formed between mushroom tyrosinase (from *Agaricus bisporus*) and the tropolone (OTR) inhibitor (PDB code: 2Y9X) was chosen as receptor [56]. Equilibrium conformer of each molecule was assessed at molecular mechanics level and optimized at PM3 level [72,73] using Spartan v.2014. The resulting structures were then optimized at the Density Functional Theory (DFT) level with Orca 5.0.4 [74,75] (PBE0 density functional [76], def2-SVP basis set [77]). The nature of the minima achieved after the optimization procedures was confirmed by the absence of negative IR frequencies in the Hessian matrix. The computational setup adopted for the molecular docking simulations was already described and validated [55]. The conformations adopted by the docked poses and their intermolecular interactions were analysed using Biovia Discovery studio viewer 2021, USCF Chimera v. 1.8 [78] and USCF ChimeraX v. 1.8 [79]. Analysis of the hydrophobic interactions was performed by colouring the surrounding residues according to the Kyte–Doolittle hydrophobicity scale values [80].

3.14. Statistical Analysis

Statistically significant differences were assessed by calculating a one-way ANOVA followed by the Tukey Multiple Comparisons Test, both using the Graph Pad INSTAT software v8.2 (GraphPad Software, San Diego, CA, USA).

4. Conclusions

In this work, we have reported the design and synthesis of a new series of tyrosinase inhibitors bearing the thiosemicarbazones fragment, by introducing the combination of para-substitution and lipophilicity-exploiting strategies. This approach enabled the development of compounds with inhibitory effects on tyrosinase significantly higher than those shown by the standard inhibitor kojic acid, highlighting their potential for treating hyperpigmentation and related skin problems. With a view to the possible dermatological use, it is worthy to remark that the synthesized thiosemicarbazones show promising photoprotective properties, with SPF values higher than those of the commonly used sunscreen agents. Importantly, cytotoxicity experiments verified the non-toxicity of our compounds at concentrations efficient for tyrosinase inhibition.

Molecular docking experiments revealed useful information about these compounds' binding interactions with the active site of mushroom tyrosinase, clarifying their mechanism of action as possible anti-tyrosinase drugs. The capability of selected compounds to chelate critical copper ions in the enzyme increases their inhibitory potency and applications.

In conclusion, the thiosemicarbazone derivatives synthesized in this study represent a promising class of compounds for potential therapeutic and cosmetic applications aimed at regulating melanin production and providing UV protection. The results obtained open promising perspectives for further in vitro studies with human tyrosinase and on cellular systems for melanogenesis studies.

Supplementary Materials: The following supporting information can be downloaded at <https://www.mdpi.com/article/10.3390/molecules29235629/s1>: Figure S1: ^1H NMR spectrum of **TC1**, (*E*)-2-(4-hydroxybenzylidene)hydrazine-1-carbothioamide (600 MHz, DMSO *d*-6); Figure S2: ^1H NMR spectrum of **TCMS1**, (*E*)-4-((2-carbamothioylhydrazineylidene)methyl)phenyl methanesulfonate (600 MHz, DMSO *d*-6); Figure S3: ^{13}C NMR spectrum of **TCMS1**, (*E*)-4-((2-carbamothioylhydrazineylidene)methyl)phenyl methanesulfonate (151 MHz, DMSO *d*-6); Figure S4: ^1H NMR spectrum of **TCBS1**, (*E*)-4-((2-carbamothioylhydrazineylidene)methyl)phenyl benzenesulfonate (600 MHz, Acetone-*d*6); Figure S5: ^{13}C NMR spectrum of **TCBS1**, (*E*)-4-((2-carbamothioylhydrazineylidene)methyl)phenyl benzenesulfonate (151 MHz, Acetone-*d*6); Figure S6: ^1H NMR spectrum of **TCBS2**, (*E*)-4-((2-carbamothioylhydrazineylidene)methyl)phenyl 4-nitrobenzenesulfonate (600 MHz, DMSO *d*-6); Figure S7: ^{13}C NMR spectrum of **TCBS2**, (*E*)-4-((2-carbamothioylhydrazineylidene)methyl)phenyl 4-nitrobenzenesulfonate (151 MHz, DMSO *d*-6); Figure S8: ^1H NMR spectrum of **TCBS3**, (*E*)-4-((2-carbamothioylhydrazineylidene)methyl)phenyl 4-methoxybenzenesulfonate (600 MHz, Acetone *d*-6); Figure S9: ^{13}C NMR spectrum of **TCBS3**, (*E*)-4-((2-carbamothioylhydrazineylidene)methyl)phenyl 4-methoxybenzenesulfonate (151 MHz, Acetone *d*-6); Figure S10: ^1H NMR spectrum of **TCBS4**, (*E*)-4-((2-carbamothioylhydrazineylidene)methyl)phenyl 4-methylbenzenesulfonate (600 MHz, Acetone *d*-6); Figure S11: ^{13}C NMR spectrum of **TCBS4**, (*E*)-4-((2-carbamothioylhydrazineylidene)methyl)phenyl 4-methylbenzenesulfonate (151 MHz, Acetone *d*-6); Figure S12: ^1H NMR spectrum of **TCBS5**, (*E*)-4-((2-carbamothioylhydrazineylidene)methyl)phenyl 4-chlorobenzenesulfonate (600 MHz, Acetone *d*-6); Figure S13: ^{13}C NMR spectrum of **TCBS5**, (*E*)-4-((2-carbamothioylhydrazineylidene)methyl)phenyl 4-chlorobenzenesulfonate (151 MHz, Acetone *d*-6); Figure S14: ^1H NMR spectrum of **TCBS5**, (*E*)-4-((2-carbamothioylhydrazineylidene)methyl)phenyl 4-chlorobenzenesulfonate after addition of D_2O (600 MHz, Acetone *d*-6); Figure S15: High-Resolution ESI mass spectrum (positive mode) of compound **TCMS1**; Figure S16: High-Resolution ESI mass spectrum (negative mode) of compound **TCMS1**; Table S1: Crystal data and structure refinement parameters for **TCBS1**; Table S2: Bond lengths (\AA) for compound **TCBS1**; Table S3: Bond angles ($^\circ$) for compound **TCBS1**; Table S4: Comparison between the mean bond distances (\AA) calculated for the thiosemicarbazone moieties in the two units in **TCBS1** and the mean values retrieved from the CSD (version 5.45 updated Mar 2024); Figure S17: Hydrogen bonding network found in the crystal structure of **TCBS1**: (a) partial view on the relative orientation between units A and B. (b,c) show the infinite hydrogen-bonded network for units A and B, respectively. Interactions are labelled according to Table S5; Table S5: Intermolecular hydrogen bonding interactions of **TCBS1**; Figure S18: Intermolecular π - π stacking interactions between tosyl groups in the crystal structure of **TCBS1**. Intercentroid distance: 3.90 \AA ; shift distance: 1.46 \AA ; plane to plane angle: 9° ; Figure S19: Partial view of the packing diagrams of **TCBS1** along the *a*- (left) and *b*-axis (right). Units A and B are depicted in light blue and green, respectively; Figure S20: Job's plot of Cu^{2+} and **TCBS4** at 310 nm (A) and 318 (B); (C) Absorption spectra collected by varying Cu^{2+} and **TCBS4** molar ratios in in PB 0.05 M, pH 6.8, 25 $^\circ\text{C}$, 1 cm optical path length; Figure S21: Uncorrected absorbance data at 310 nm (A) and 318 nm (B) recorded by varying Cu^{2+} and **TCBS4** molar ratios; Figure S22: Docked pose of **TC1** in the MTa site and intermolecular interactions with the surrounding residues. Hydrogen bonds are represented using light blue solid lines, while metal coordinating bonds are shown as violet dashed ones (A). π - π interaction between the docked pose of **TC1** and the Hys-263 residue; Figure S23: Docked poses of **TCMS1** (A), **TCBS1-5** (B-F) in the MTa site and intermolecular interactions with the surrounding residues. Hydrogen bonds are represented using light blue solid lines, while metal coordinating bonds are shown as violet dashed ones; Figure S24: Hydrophobic interaction analysis between the docked poses of **TC1** (A), **TCMS1** (B), **TCBS1-5** (C-G) and the surrounding residues of mushroom tyrosinase (MTa site). The aminoacidic residues are coloured according to the Kyte-Doolittle hydrophobicity scale values; Table S6: Scores, molecular interactions and distances between the highest-rated docked poses of compounds **TC1**, **TCMS1**, **TCBS1-5** and the surrounding residues of mushroom tyrosinase (MTa).

Author Contributions: Conceptualization, T.P., A.F., S.M., M.G.C. and B.E.; methodology, T.P., A.F., B.E., F.P. (Francesca Pintus), S.M., M.G.C. and F.P. (Francesca Pettinau); validation, T.P. and A.F.; formal analysis, T.P., A.F., B.E., F.P. (Francesca Pintus), S.F., E.P., S.M. and F.P. (Francesca Pettinau); investigation, T.P., A.F., B.E., S.F., E.P., F.M., S.M., M.G.C. and F.P. (Francesca Pettinau); resources T.P. and A.F.; data curation, T.P. and A.F.; writing—original draft preparation, T.P., A.F., B.E. and S.M.; writing—review and editing, T.P., A.F., B.E., S.F., F.P. (Francesca Pintus), S.M. and M.G.C.; visualization, T.P., A.F., S.M., E.P. and F.P. (Francesca Pettinau); supervision, T.P., A.F., S.M. and

M.G.C.; project administration, T.P. and A.F.; funding acquisition, T.P. and A.F. All authors have read and agreed to the published version of the manuscript.

Funding: This research received no external funding.

Institutional Review Board Statement: Not applicable.

Informed Consent Statement: Not applicable.

Data Availability Statement: Data are present within the article.

Acknowledgments: The authors thank the CeSAR (Centro Servizi Ricerca d'Ateneo) core facility of the University of Cagliari for the SC-X-ray diffraction measurements, performed with the Bruker D8 Venture diffractometer. We acknowledge Sandrina Lampis and Giulio Ferino of the CeSAR core facility for the NMR and HRMS measurements.

Conflicts of Interest: The authors declare no conflicts of interest.

References

1. Lobana, T.S. Activation of C-H Bonds of Thiosemicarbazones by Transition Metals: Synthesis, Structures and Importance of Cyclometallated Compounds. *RSC Adv.* **2015**, *5*, 37231–37274. [[CrossRef](#)]
2. Gupta, S.; Singh, N.; Khan, T.; Joshi, S. Thiosemicarbazone Derivatives of Transition Metals as Multi-Target Drugs: A Review. *Results Chem.* **2022**, *4*, 100459. [[CrossRef](#)]
3. Haldys, K.; Latajka, R. Thiosemicarbazones with Tyrosinase Inhibitory Activity. *MedChemComm* **2019**, *10*, 378–389. [[CrossRef](#)] [[PubMed](#)]
4. Li, J.; Feng, L.; Liu, L.; Wang, F.; Ouyang, L.; Zhang, L.; Hu, X.; Wang, G. Recent Advances in the Design and Discovery of Synthetic Tyrosinase Inhibitors. *Eur. J. Med. Chem.* **2021**, *224*, 113744. [[CrossRef](#)] [[PubMed](#)]
5. Peng, Z.; Wang, G.; Zeng, Q.H.; Li, Y.; Liu, H.; Wang, J.J.; Zhao, Y. A Systematic Review of Synthetic Tyrosinase Inhibitors and Their Structure-Activity Relationship. *Crit. Rev. Food Sci. Nutr.* **2021**, *62*, 4053–4094. [[CrossRef](#)] [[PubMed](#)]
6. Zolghadri, S.; Bahrami, A.; Hassan Khan, M.T.; Munoz-Munoz, J.; Garcia-Molina, F.; Garcia-Canovas, F.; Saboury, A.A. A Comprehensive Review on Tyrosinase Inhibitors. *J. Enzym. Inhib. Med. Chem.* **2019**, *34*, 279–309. [[CrossRef](#)]
7. Ledwoń, P.; Goldeman, W.; Haldys, K.; Jewgiński, M.; Calamai, G.; Rossowska, J.; Papini, A.M.; Rovero, P.; Latajka, R. Tripeptides Conjugated with Thiosemicarbazones: New Inhibitors of Tyrosinase for Cosmeceutical Use. *J. Enzym. Inhib. Med. Chem.* **2023**, *38*, 2193676. [[CrossRef](#)]
8. Hosseinpour, H.; Moghadam Farid, S.; Iraj, A.; Askari, S.; Edraki, N.; Hosseini, S.; Jamshidzadeh, A.; Larijani, B.; Attaroshan, M.; Pirhadi, S.; et al. Anti-Melanogenesis and Anti-Tyrosinase Properties of Aryl-Substituted Acetamides of Phenoxy Methyl Triazole Conjugated with Thiosemicarbazide: Design, Synthesis and Biological Evaluations. *Bioorganic Chem.* **2021**, *114*, 104979. [[CrossRef](#)]
9. Slominski, A.; Tobin, D.J.; Shibahara, S.; Wortsman, J. Melanin Pigmentation in Mammalian Skin and Its Hormonal Regulation. *Physiol. Rev.* **2004**, *84*, 1155–1228. [[CrossRef](#)]
10. De Luca, L.; Germanò, M.P.; Fais, A.; Pintus, F.; Buemi, M.R.; Vittorio, S.; Mirabile, S.; Rapisarda, A.; Gitto, R. Discovery of a New Potent Inhibitor of Mushroom Tyrosinase (*Agaricus Bisporus*) Containing 4-(4-Hydroxyphenyl)Piperazin-1-Yl Moiety. *Bioorg. Med. Chem.* **2020**, *28*, 115497. [[CrossRef](#)] [[PubMed](#)]
11. Era, B.; Floris, S.; Sogos, V.; Porcedda, C.; Piras, A.; Medda, R.; Fais, A.; Pintus, F. Anti-Aging Potential of Extracts from *Washingtonia Filifera* Seeds. *Plants* **2021**, *10*, 151. [[CrossRef](#)]
12. Baber, M.A.; Crist, C.M.; Devolve, N.L.; Patrone, J.D. Tyrosinase Inhibitors: A Perspective. *Molecules* **2023**, *28*, 5762. [[CrossRef](#)]
13. Haudecoeur, R.; Gouron, A.; Dubois, C.; Lightbody, M. Investigation of Binding-Site Homology between Mushroom and Bacterial Tyrosinases by Using Aurones as Effectors. *ChemBioChem* **2014**, *15*, 1325–1333. [[CrossRef](#)]
14. Fogal, S.; Carotti, M.; Giaretta, L.; Lanciai, F.; Nogara, L.; Bubacco, L.; Bergantino, E. Human Tyrosinase Produced in Insect Cells: A Landmark for the Screening of New Drugs Addressing Its Activity. *Mol. Biotechnol.* **2015**, *57*, 45–57. [[CrossRef](#)]
15. Mann, T.; Gerwat, W.; Batzer, J.; Eggers, K.; Scherner, C.; Wenck, H. Inhibition of Human Tyrosinase Requires Molecular Motifs Distinctively Different from Mushroom Tyrosinase. *J. Invest. Dermatol.* **2018**, *138*, 1601–1608. [[CrossRef](#)]
16. Chandarajoti, K.; Kara, J.; Suwanhom, P.; Nualnoi, T.; Puripattanavong, J.; Lee, V.S.; Tipmanee, V. Synthesis and Evaluation of Coumarin Derivatives on Antioxidative, Tyrosinase Inhibitory Activities, Melanogenesis, and in Silico Investigations. *Sci. Rep.* **2024**, *14*, 5535. [[CrossRef](#)]
17. Soares, M.A.; Almeida, M.A.; Marins-Goulart, C.; Chaves, O.A.; Echevarria, A.; de Oliveira, M.C.C. Thiosemicarbazones as Inhibitors of Tyrosinase Enzyme. *Bioorg. Med. Chem. Lett.* **2017**, *27*, 3546–3550. [[CrossRef](#)]
18. Haldys, K.; Goldeman, W.; Jewgiński, M.; Wolińska, E.; Anger-Góra, N.; Rossowska, J.; Latajka, R. Halogenated Aromatic Thiosemicarbazones as Potent Inhibitors of Tyrosinase and Melanogenesis. *Bioorg. Chem.* **2020**, *94*, 103419. [[CrossRef](#)]
19. Hosseinpour, H.; Iraj, A.; Edraki, N.; Pirhadi, S.; Attaroshan, M.; Khoshneviszadeh, M.; Khoshneviszadeh, M. A Series of Benzylidenes Linked to Hydrazine-1-Carbothioamide as Tyrosinase Inhibitors: Synthesis, Biological Evaluation and Structure—Activity Relationship. *Chem. Biodivers.* **2020**, *17*, e2000285. [[CrossRef](#)]

20. Yi, W.; Cao, R.H.; Chen, Z.Y.; Yu, L.; Ma, L.; Song, H.C. Design, Synthesis and Biological Evaluation of Hydroxy- or Methoxy-Substituted Phenylmethylenethiosemicarbazones as Tyrosinase Inhibitors. *Chem. Pharm. Bull.* **2009**, *57*, 1273–1277. [[CrossRef](#)] [[PubMed](#)]
21. Lee, K.C.; Thanigaimalai, P.; Sharma, V.K.; Kim, M.S.; Roh, E.; Hwang, B.Y.; Kim, Y.; Jung, S.H. Structural Characteristics of Thiosemicarbazones as Inhibitors of Melanogenesis. *Bioorg. Med. Chem. Lett.* **2010**, *20*, 6794–6796. [[CrossRef](#)] [[PubMed](#)]
22. Kaur, R.; Kumar, R.; Dogra, N.; Yadav, A.K. Design, Synthesis, Biological Evaluations and in Silico Studies of Sulfonate Ester Derivatives of 2-(2-Benzylidenehydrazono)Thiazolidin-4-One as Potential α -Glucosidase Inhibitors. *J. Mol. Struct.* **2022**, *1247*, 131266. [[CrossRef](#)]
23. Tokali, F.S.; Taslimi, P.; Tüzün, B.; Karakuş, A.; Sadeghian, N.; Gulçin, İ. Synthesis of New Carboxylates and Sulfonates Containing Thiazolidin-4-One Ring and Evaluation of Inhibitory Properties against Some Metabolic Enzymes. *J. Iran. Chem. Soc.* **2023**, *20*, 2631–2642. [[CrossRef](#)]
24. Cao, S.; Wang, D.; Cheng, R.; Shi, W.; Zhang, Q.; Zeng, H.; Chen, J.; Zhang, E.Q.; Zeng, H.; Chen, J. Spectrochimica Acta Part A: Molecular and Biomolecular Spectroscopy Modulation of the Lipophilicity and Molecular Size of Thiosemicarbazone Inhibitors to Regulate Tyrosinase Activity. *Spectrochim. Acta Part A Mol. Biomol. Spectrosc.* **2022**, *281*, 121590. [[CrossRef](#)] [[PubMed](#)]
25. Leblanc, M.; Gonzalez-sarr, A.; Beckford, F.A.; Mbarushimana, P.C.; Seeram, N.P. Coordination Chemistry of Polyaromatic Thiosemicarbazones 2: Synthesis and Biological Activity of Zinc, Cobalt, and Copper Complexes of 1-(Naphthalene-2-Yl) Ethanone Thiosemicarbazone. *Int. J. Inorg. Chem.* **2011**, *2011*, 624756. [[CrossRef](#)]
26. Schäfer, M.; Drayß, M.; Springer, A.; Zacharias, P.; Meerholz, K. Radical Cations in Electrospray Mass Spectrometry: Formation of Open-Shell Species, Examination of the Fragmentation Behaviour in ESI-MSn and Reaction Mechanism Studies by Detection of Transient Radical Cations. *Eur. J. Org. Chem.* **2007**, *31*, 5162–5174. [[CrossRef](#)]
27. Iftikhar, I.; Brajter-Toth, A. Solution or Gas Phase? Oxidation and Radical Formation in Electrospray Ionization Mass Spectrometry (ESI MS). *Electroanalysis* **2015**, *27*, 2872–2881. [[CrossRef](#)]
28. Morand, K.; Talbo, G.; Mann, M. Oxidation of Peptides during Electrospray Ionization. *Rapid Commun. Mass Spectrom.* **1993**, *7*, 738–743. [[CrossRef](#)]
29. Sojo, L.E.; Chahal, N.; Keller, B.O. Oxidation of Catechols during Positive Ion Electrospray Mass Spectrometric Analysis: Evidence for in-Source Oxidative Dimerization. *Rapid Commun. Mass Spectrom.* **2014**, *28*, 2181–2190. [[CrossRef](#)]
30. Hao, C.; March, R.E. Electrospray Ionization Tandem Mass Spectrometric Study of Salt Cluster Ions: Part 2—Salts of Polyatomic Acid Groups and of Multivalent Metals. *J. Mass Spectrom.* **2001**, *36*, 509–521. [[CrossRef](#)]
31. Masuri, S.; Cadoni, E.; Cabiddu, M.G.; Isaia, F.; Demuru, M.G.; Morán, L.; Morán, L.; Bucek, D.; Vanhara, P.; Vanhara, P.; et al. The First Copper(II) Complex with 1,10-Phenanthroline and Salubrial with Interesting Biochemical Properties. *Metallomics* **2020**, *12*, 891–901. [[CrossRef](#)] [[PubMed](#)]
32. Etter, M.C.; MacDonald, J.C.; Bernstein, J. Graph-Set Analysis of Hydrogen-Bond Patterns in Organic Crystals. *Acta Cryst.* **1990**, *B46*, 256–262. [[CrossRef](#)] [[PubMed](#)]
33. Spackman, M.A.; Jayatilaka, D. Hirshfeld Surface Analysis. *Cryst. Eng. Comm.* **2009**, *11*, 19–32. [[CrossRef](#)]
34. McKinnon, J.J.; Fabbiani, F.P.A.; Spackman, M.A. Hirshfeld Surface Analysis 2007. *Cryst. Growth Des.* **2007**, *7*, 55–76.
35. McKinnon, J.J.; Spackman, M.A.; Mitchell, A.S. Novel Tools for Visualizing and Exploring Intermolecular Interactions in Molecular Crystals. *Acta Cryst.* **2004**, *B60*, 627–668. [[CrossRef](#)] [[PubMed](#)]
36. Luo, Y.; Wu, G.; Mao, S.; Sun, B. Inorganica Chimica Acta Complexation of Different Metals with a Novel N-Donor Bridging Receptor and Hirshfeld Surfaces Analysis. *Inorganica Chim. Acta* **2013**, *397*, 1–9. [[CrossRef](#)]
37. Şahin, S.; Dege, N. Hirshfeld Surface, ADMET, Boiled-Egg Model Properties and Molecular Docking Studies with Human Cyclophilin D (CypD) of a Schiff Base Methanimine. *Polyhedron* **2021**, *205*, 115320. [[CrossRef](#)]
38. Allali, M.; Dege, N.; Karrouchi, K.; Benchat, N. Synthesis, Spectroscopy, Crystal Structure, TGA/DTA Study, DFT and Molecular Docking Investigations of (E)-4-(4-Methylbenzyl)-6-Styrylpyridazin-3(2H)-One. *J. Mol. Struct.* **2021**, *1228*, 129435. [[CrossRef](#)]
39. Yuan, F.; Zhang, R.; Qiao, C.; Luo, X.; Zhou, C. Series of Ln-Metal Organic Frameworks: Photocatalytic Performance and Hirshfeld Surface Analyses. *J. Mol. Struct.* **2022**, *1251*, 131956. [[CrossRef](#)]
40. Pinto, C.B.; Dos Santos, L.H.R.; Rodrigues, B.L. Understanding Metal—Ligand Interactions in Coordination Polymers Using Hirshfeld Surface Analysis Research Papers. *Crystallogr. Sect. C Struct. Chem.* **2019**, *75*, 707–716. [[CrossRef](#)]
41. Turner, M.J.; Grabowsky, S.; Jayatilaka, D.; Spackman, M.A. Accurate and Efficient Model Energies for Exploring Intermolecular Interactions in Molecular Crystals. *J. Phys. Chem. Lett.* **2014**, *5*, 4249–4255. [[CrossRef](#)] [[PubMed](#)]
42. Dege, N.; Asam, M.; Onur, R.; Doğan, E.; Açar, T.; Waseem, M. Theoretical and Experimental Approaches of New Schiff Bases: Efficient Synthesis, X-Ray Structures, DFT, Molecular Modeling and ADMET Studies. *J. Iran. Chem. Soc.* **2021**, *18*, 2345–2368. [[CrossRef](#)]
43. Turner, M.J.; McKinnon, J.J.; Jayatilaka, D.; Spackman, M.A. Visualisation and Characterisation of Voids in Crystalline Materials. *CrystEngComm* **2011**, *13*, 1804. [[CrossRef](#)]
44. Irrou, E.; Elmachkouri, A.; Mazzah, A.; Ho, T. Crystal Structure, Hirshfeld Surface and Crystal Void Analysis, Intermolecular Interaction Energies, DFT Calculations and Energy Frameworks of 2H-Benzo[b][1,4]Thiazin-3(4H)-One 1, 1-Dioxide. *Acta Cryst.* **2023**, *3*, 1037–1043. [[CrossRef](#)] [[PubMed](#)]
45. Lipinski, C.A.; Lombardo, F.; Dominy, B.W.; Feeney, P.J. Experimental and Computational Approaches to Estimate Solubility and Permeability in Drug Discovery and Development Settings. *Adv. Drug Deliv. Rev.* **2012**, *64*, 4–17. [[CrossRef](#)]

46. Ertl, P.; Rohde, B.; Selzer, P. Fast Calculation of Molecular Polar Surface Area as a Sum of Fragment-Based Contributions and Its Application to the Prediction of Drug Transport Properties. *J. Med. Chem.* **2000**, *43*, 3714–3717. [[CrossRef](#)]
47. Pajouhesh, H.; Lenz, G.R. Medicinal Chemical Properties of Successful Central Nervous System Drugs. *NeuroRX* **2005**, *2*, 541–553. [[CrossRef](#)]
48. Matos, M.J.; Varela, C.; Vilar, S.; Hripcsak, G.; Borges, F.; Santana, L.; Uriarte, E.; Fais, A.; Di Petrillo, A.; Pintus, F.; et al. Design and Discovery of Tyrosinase Inhibitors Based on a Coumarin Scaffold. *RSC Adv.* **2015**, *5*, 94227–94235. [[CrossRef](#)]
49. Rajnochová Svobodová, A.; Gabrielová, E.; Michaelides, L.; Kosina, P.; Ryšavá, A.; Ulrichová, J.; Zálešák, B.; Vostálová, J. UVA-Photoprotective Potential of Silymarin and Silybin. *Arch. Dermatol. Res.* **2018**, *310*, 413–424. [[CrossRef](#)]
50. Han, B.; Weatherley, A.J.; Mumford, K.; Bolan, N.; He, J.Z.; Stevens, G.W.; Chen, D. Modification of Naturally Abundant Resources for Remediation of Potentially Toxic Elements: A Review. *J. Hazard. Mater.* **2022**, *421*, 126755. [[CrossRef](#)]
51. Masuri, S.; Cabiddu, M.G.; Moráň, L.; Vesselá, T.; Bartosik, M.; Havel, J.; Meloni, F.; Cadoni, E.; Vaňhara, P.; Pivetta, T. Ternary Copper(II) Complexes of 1,10-Phenanthroline and Coumarin-Based Oxylacetates as pro-Apoptotic UPR CHOP Inducers. *New J. Chem.* **2023**, *47*, 15125–15136. [[CrossRef](#)]
52. Moráň, L.; Pivetta, P.; Masuri, S.; Vašičková, K.; Walter, F.; Prehn, J.; Elkalf, M.; Trnka, J.; Havel, J.; Vaňhara, P. Mixed Copper(II)–Phenanthroline Complexes Induce Cell Death of Ovarian Cancer Cells by Evoking the Unfolded Protein Response. *Metallomics* **2019**, *11*, 1481–1489. [[CrossRef](#)] [[PubMed](#)]
53. Sîrbu, A.; Palamarcu, O.; Babak, M.V.; Lim, J.M.; Ohui, K.; Eryedy, E.A.; Shova, S.; Darvasiová, D.; Rapta, P.; Ang, W.H.; et al. Copper(II) Thiosemicarbazone Complexes Induce Marked ROS Accumulation and Promote Nrf2-Mediated Antioxidant Response in Highly Resistant Breast Cancer Cells. *Dalton Trans.* **2017**, *46*, 3833–3847. [[CrossRef](#)] [[PubMed](#)]
54. Mutlu Gençkal, H.; Erkisa, M.; Alper, P.; Sahin, S.; Ulukaya, E.; Ari, F. Mixed Ligand Complexes of Co(II), Ni(II) and Cu(II) with Quercetin and Diimine Ligands: Synthesis, Characterization, Anti-Cancer and Anti-Oxidant Activity. *J. Biol. Inorg. Chem.* **2020**, *25*, 161–177. [[CrossRef](#)]
55. Masuri, S.; Era, B.; Pintus, F.; Cadoni, E.; Cabiddu, M.G.; Fais, A.; Pivetta, T. Hydroxylated Coumarin-Based Thiosemicarbazones as Dual Antityrosinase and Antioxidant Agents. *Int. J. Mol. Sci.* **2023**, *24*, 1678. [[CrossRef](#)]
56. Ismaya, W.T.; Rozeboom, H.J.; Weijn, A.; Mes, J.J.; Fusetti, F.; Wichers, H.J.; Dijkstra, B.W. Crystal Structure of Agaricus Bisporus Mushroom Tyrosinase: Identity of the Tetramer Subunits and Interaction with Tropolone. *Biochemistry* **2011**, *50*, 5477–5486. [[CrossRef](#)]
57. Roselan, M.A.; Zakaria, N.; Faujan, N.H.; Mohammad Latif, M.A.; Mohd Faudzi, S.M.; Ab Hadi, H.; Ashari, S.E. In Vitro Cytotoxicity Assay, Mushroom Tyrosinase Inhibitory Activity and Release Analysis of Kojic Monooleate Nanodelivery System and in Silico Molecular Docking Study against 2Y9X Target Enzyme. *J. Drug Deliv. Sci. Technol.* **2021**, *66*, 102764. [[CrossRef](#)]
58. Singh, L.R.; Chen, Y.L.; Xie, Y.Y.; Xia, W.; Gong, X.W.; Hider, R.C.; Zhou, T. Functionality Study of Chalcone-Hydroxypyridinone Hybrids as Tyrosinase Inhibitors and Influence on Anti-Tyrosinase Activity. *J. Enzym. Inhib. Med. Chem.* **2020**, *35*, 1562–1567. [[CrossRef](#)]
59. Alizadeh, N.; Hossein, M.; Iraj, A.; Yazzaf, R.; Moazzam, A. Bioorganic Chemistry Evaluating the Effects of Disubstituted 3-Hydroxy-1H-Pyrrol-2(5H)-One Analog as Novel Tyrosinase Inhibitors. *Bioorg. Chem.* **2022**, *126*, 105876. [[CrossRef](#)]
60. Haldys, K.; Goldeman, W.; Anger-Góra, N.; Rossowska, J.; Latajka, R. Monosubstituted Acetophenone Thiosemicarbazones as Potent Inhibitors of Tyrosinase: Synthesis, Inhibitory Studies, and Molecular Docking. *Pharmaceuticals* **2021**, *14*, 74. [[CrossRef](#)]
61. Pivetta, T.; Masuri, S.; Cabiddu, M.G.; Caltagirone, C.; Pintus, A.; Massa, M.; Isaia, F.; Cadoni, E. A Novel Ratiometric and Turn-on Fluorescent Coumarin-Based Probe for Fe(III). *New J. Chem.* **2019**, *43*, 12032–12041. [[CrossRef](#)]
62. Niedermeyer, T.H.J.; Strohal, M. MMass as a Software Tool for the Annotation of Cyclic Peptide Tandem Mass Spectra. *PLoS ONE* **2012**, *7*, e0044913. [[CrossRef](#)] [[PubMed](#)]
63. Strohal, M.; Kavan, D.; Novák, P.; Volný, M.; Havlíček, V. MMass 3: A Cross-Platform Software Environment for Precise Analysis of Mass Spectrometric Data. *Anal. Chem.* **2010**, *82*, 4648–4651. [[CrossRef](#)]
64. Denziel, R.; Ajamian, A. Inhibitors of Histone Deacetylase and Prodrugs Thereof 2008. United. States Patent US 8,796,330, 5 August 2014.
65. Da Silva, J.B.P.; Navarro, D.M.D.A.F.; Da Silva, A.G.; Santos, G.K.N.; Dutra, K.A.; Moreira, D.R.; Ramos, M.N.; Espíndola, J.W.P.; De Oliveira, A.D.T.; Brondani, D.J.; et al. Thiosemicarbazones as Aedes Aegypti Larvicidal. *Eur. J. Med. Chem.* **2015**, *100*, 162–175. [[CrossRef](#)]
66. Sheldrick, G.M. SHELXT—Integrated Space-Group and Crystal-Structure Determination. *Acta Crystallogr. Sect. A Found. Crystallogr.* **2015**, *71*, 3–8. [[CrossRef](#)]
67. Dolomanov, O.V.; Bourhis, L.J.; Gildea, R.J.; Howard, J.A.K.; Puschmann, H. OLEX2: A Complete Structure Solution, Refinement and Analysis Program. *J. Appl. Crystallogr.* **2009**, *42*, 339–341. [[CrossRef](#)]
68. Yi, W.; Wu, X.; Cao, R.; Song, H.; Ma, L. Biological Evaluations of Novel Vitamin C Esters as Mushroom Tyrosinase Inhibitors and Antioxidants. *Food Chem.* **2009**, *117*, 381–386. [[CrossRef](#)]
69. Sayre, R.M.; Po Ha Gin, P.; Levee, G.J.; Marlowe, E. A Comparison of in Vivo and in Vitro Testing of Sunscreening Formulas. *Photochem. Photobiol.* **1979**, *29*, 559–566. [[CrossRef](#)]
70. Pintus, F.; Floris, S.; Fais, A.; Era, B.; Kumar, A.; Gatto, G.; Uriarte, E.; Matos, M.J. Hydroxy-3-Phenylcoumarins as Multitarget Compounds for Skin Aging Diseases: Synthesis, Molecular Docking and Tyrosinase, Elastase, Collagenase and Hyaluronidase Inhibition, and Sun Protection Factor. *Molecules* **2022**, *27*, 6914. [[CrossRef](#)]

71. Jones, G.; Willett, P.; Glen, R.C.; Leach, A.R.; Taylor, R. Development and Validation of a Genetic Algorithm for Flexible Docking. *J. Mol. Biol.* **1997**, *267*, 727–748. [[CrossRef](#)]
72. Stewart, J.J.P. Optimization of Parameters for Semiempirical Methods I. Method. *J. Comput. Chem.* **1989**, *10*, 209–220. [[CrossRef](#)]
73. Stewart, J.J.P. Optimization of Parameters for Semiempirical Methods II. Applications. *J. Comput. Chem.* **1989**, *10*, 221–264. [[CrossRef](#)]
74. Neese, F. The ORCA Program System. *WIREs Comput. Mol. Sci.* **2012**, *2*, 73–78. [[CrossRef](#)]
75. Neese, F. Software Update: The ORCA Program System—Version 5.0. *Wiley Interdiscip. Rev. Comput. Mol. Sci.* **2022**, *12*, e1606. [[CrossRef](#)]
76. Adamo, C.; Barone, V. Toward Reliable Density Functional Methods without Adjustable Parameters: The PBE0 Model. *J. Chem. Phys.* **1999**, *110*, 6158–6170. [[CrossRef](#)]
77. Weigend, F.; Ahlrichs, R.; Gmbh, F.K. Balanced Basis Sets of Split Valence, Triple Zeta Valence and Quadruple Zeta Valence Quality for H to Rn: Design and Assessment of Accuracy. *W. Phys. Chem. Chem. Phys.* **2005**, *7*, 3297–3305. [[CrossRef](#)]
78. Pettersen, E.F.; Goddard, T.D.; Huang, C.C.; Couch, G.S.; Greenblatt, D.M.; Meng, E.C.; Ferrin, T.E. UCSF Chimera—A Visualization System for Exploratory Research and Analysis. *J. Comput. Chem.* **2004**, *25*, 1605–1612. [[CrossRef](#)]
79. Meng, E.C.; Goddard, T.D.; Pettersen, E.F.; Couch, G.S.; Pearson, Z.J.; Morris, J.H.; Ferrin, T.E. UCSF ChimeraX: Tools for Structure Building and Analysis. *Protein Sci.* **2023**, *32*, e4792. [[CrossRef](#)] [[PubMed](#)]
80. Kyte, J.; Doolittle, R.F.; Diego, S.; Jolla, L. A Simple Method for Displaying the Hydrophobic Character of a Protein. *J. Mol. Biol.* **1982**, *157*, 105–132. [[CrossRef](#)]

Disclaimer/Publisher’s Note: The statements, opinions and data contained in all publications are solely those of the individual author(s) and contributor(s) and not of MDPI and/or the editor(s). MDPI and/or the editor(s) disclaim responsibility for any injury to people or property resulting from any ideas, methods, instructions or products referred to in the content.